Dependence of NO Recombination Dynamics in Horse Myoglobin on Solution Glycerol Content

Andrew P. Shreve,* Stefan Franzen,‡ M. Cather Simpson,§ and R. Brian Dyer

CST-4, MS G755, Bioscience and Biotechnology Group, Los Alamos National Laboratory, Los Alamos, New Mexico 87545

Received: April 6, 1999; In Final Form: June 21, 1999

The recombination dynamics of NO with horse heart myoglobin (Mb) following photolysis with a 570 nm excitation pulse were measured by time-resolved absorption with 250 fs temporal resolution. These measurements were carried out in room-temperature solutions in which the glycerol concentration was varied from 0 to 90% (w/v). The recombination of NO is nonsingle exponential in all cases, but becomes faster as the glycerol concentration is increased. The interpretation of these results is aided by a maximum entropy analysis to determine a distribution of rate processes consistent with the data. This analysis suggests that in buffer there are two dominant rate processes for NO recombination on the subnanosecond time scale, one at ≈10 ps and one at ≈200 ps. The dominant effect of increasing glycerol content is to increase the amplitude of the fast process, with no corresponding significant change in rate, and to decrease the amplitude of the slow process, but with a corresponding increase in rate. These results are consistent with a photodissociation process in which photolyzed NO partitions immediately between two distinct populations, one of which has a rapid and the other of which has a slower recombination. The rate of the rapid recombination is independent of glycerol concentration, and therefore decoupled from any protein relaxation process influenced by glycerol, while that of the slower recombination increases at higher glycerol concentration. Further, the partitioning between these two populations also depends on glycerol content, with the relative amplitude of the faster recombination process increasing as the glycerol content is increased. Interpretation of these observations in terms of ligand trajectories following photodissociation, and possible connections of these results with both infrared and crystallographic studies of photodissociated MbCO are discussed.

1. Introduction

The recombination of small diatomic ligands with the heme prosthetic group in myoglobin (Mb) following photolysis has served as a model reaction for the study of protein dynamics for many decades.[1−4] Even after such extensive study, controversy remains as to the factors that control this conceptually simple reaction. A clear result, however, is that the rebinding of diatomic ligands can be strongly coupled to motions of the protein. For example, in the case of CO, there are two distinct phases of ligand rebinding. The faster geminate phase occurs with ≈4% yield on the submicrosecond time scale in room-temperature solutions and involves the rebinding of photolyzed CO molecules prior to their escape from the protein into the solvent.[1] The slower phase involves the recombination of CO molecules after their escape into solution, demonstrates bimolecular kinetics, and occurs on the millisecond time scale for the protein and CO concentrations normally studied. The study of the kinetics of geminate recombination can probe the coupling of protein motions to geminate recombination processes, and many experiments of this type have been performed to address the nature of the underlying protein dynamics that control ligand recombination. However, in room-temperature buffer solution, the small yield for CO geminate recombination implies that the observed rate of this process is dominated by the rate constant for ligand escape from the protein rather than by the rate constant for ligand recombination to the heme group.[1] For this reason, experiments that address the control of CO recombination by protein dynamics are usually performed under experimental conditions, such as low temperature or elevated solution viscosity, that significantly increase the yield of the geminate process.

For other diatomic ligands, the situation is different. In the case of O_2, a fast recombination process occurs within picoseconds of photolysis, and in room-temperature solution, the relative amplitude of this fast process is ≈30%.[5,6] The dynamics for the recombination of the remaining O_2 molecules are distributed over a wide range of time scales, and a significant fraction of these molecules eventually escape to the solvent and are then subject to the usual bimolecular recombination processes. Although O_2 is the physiologically important ligand for Mb, studies of recombination dynamics in MbO_2 are complicated by a propensity for protein degradation by autoxidation. An attractive alternative for ligand recombination studies is thus NO, because NO also demonstrates fast, large amplitude, ligand recombination on the picosecond time scale, has a near unity yield for geminate recombination, and is not subject to autoxidation difficulties.[7−9]

In this work, we examine how the glycerol content of the buffer solution affects NO recombination to the heme in Mb at room temperature. This work was motivated by two previous observations. First, for the case of NO rebinding at room

* To whom correspondence should be addressed. E-mail: shreve@lanl.gov.
§ Current address: Department of Chemistry, Case Western Reserve University, Cleveland, Ohio 44106.
‡ Current address: Department of Chemistry, North Carolina State University, Raleigh, North Carolina 27695.

10.1021/jp991163g CCC: $18.00
Published on Web 08/27/1999

temperature in pure buffer (no glycerol present), the time scales of the fast rebinding processes are qualitatively similar to the time scales of protein relaxation processes. The latter can be measured, for example, by monitoring the relaxation following photodissociation of spectral shifts of the so-called band III iron−porphyrin charge-transfer electronic absorption[10] or time-dependent changes in the protein amide I infrared (IR) absorption.[11] This correspondence of time scales suggests the possibility that the ultrafast rebinding processes are also coupled to protein relaxations. Second, the addition of glycerol can slow protein relaxation processes, as reflected, for example, in the time-dependence of the magnitude of band III spectral shifts.[12] Specifically, at ambient temperature and for any given time during the relaxation following ligand photodissociation, the magnitude of the band III spectral shift relative to its equilibrium position is larger in glycerol-containing solutions than in pure buffer solutions, suggesting that the relaxation toward equilibrium is significantly slower in the glycerol solutions.[10,12] (No glycerol-dependent studies of dynamics of the protein amide I IR band following ligand photodissociation have been done at room temperature.) Therefore, an interesting question is whether this slowing of protein relaxation will influence the ultrafast rebinding processes of NO.

We report that although the addition of substantial glycerol to the protein solution does have an influence on the subnanosecond rebinding processes of NO, this influence is relatively subtle. Upon photolysis at room temperature, we find that an immediate branching occurs, following which some fraction of the dissociated NO molecules recombine with a fast rate, while most of the remainder recombine with a significantly slower rate, all on the subnanosecond time scale. When glycerol is added to the solution, the amplitude of the fast rebinding process increases with no corresponding change in its rate, whereas the slower process becomes both slightly faster and carries a lower amplitude. Interpretation of these results is presented in terms of two recently observed spectroscopically distinct states (B states) of photodissociated MbNO at low temperature.[13] This interpretation leads to the conclusion (vide infra) that added glycerol slightly increases the rate of interconversion of the two B states, probably as a result of a slowing of protein relaxation, but the ultrafast rebinding rate of the B_1 state is independent of glycerol concentration and therefore uncoupled from those protein relaxation processes that contribute to band III spectral shifts.

2. Experimental Section

Horse-heart Mb was purchased from Sigma and prepared using a standard procedure. Myoglobin was dissolved in 50 mM phosphate buffer at pH 7.0, reduced with dithionite, and exposed under oxygen-free conditions to 1 atm of NO. For some experiments, as noted, deoxygenated glycerol was added to the sample to obtain the desired weight/volume percentage of glycerol in buffer. A major effect of added glycerol is to increase the solvent viscosity (from ≈1 cP in buffer to ≈200 cP at 90% w/v glycerol[14]); however, glycerol addition is also capable of changing the internal hydration state of proteins.[15] After binding of NO, the MbNO sample was transferred under an argon atmosphere to a gastight sample cell (1 mm optical path) in which the experiments were performed. All experiments were performed at ambient laboratory temperature (21 ± 1 °C).

The laser system used for these experiments consists of a Ti:sapphire regenerative amplifier that produces 180 fs pulses at 810 nm, each containing ∼550 μJ of energy, with a pulse repetition rate of 1 kHz. A portion of each 810 nm pulse is directed into a home-built optical parametric amplifier, which generates tunable signal and idler output in the 1.1−2.4 μm spectral range. For the experiments described here, 570 nm pump light was generated by tuning the optical parametric amplifier to generate an idler pulse at 1.92 μm and sum-frequency mixing this pulse with a portion of the 810 nm regenerative amplifier output. The resulting 570 nm pump pulse contained ≈3 μJ of energy. Probe light was generated by taking a small portion of the 810 nm regenerative amplifier output, passing it through an optical delay line, and then focusing it tightly into a 2 mm thick sapphire plate. The resulting white light continuum was filtered to retain only the blue spectral region. The pump and probe pulses were focused together into the sample, and the transmitted probe pulse was directed into a scanning monochromator and detected at the output. Pump-on minus pump-off difference spectra were obtained by chopping the 570 nm pump pulse train while monitoring the output of a lock-in amplifier whose input was the probe pulse signal. To obtain transient spectra, the time delay between the pump and probe was fixed and the wavelength of the detection monochromator was scanned, whereas to obtain kinetic data, the wavelength of the detection monochromator was held fixed and the optical delay line was scanned. Transient spectral data could be obtained using probe wavelengths as low as 400 nm, though careful optimization of the continuum generation was required to yield probe light of the required stability at these low wavelengths, and there is interference from low-yield second harmonic generation of the Ti:sapphire input at wavelengths between 400 and 410 nm. All the transient data reported here were obtained using 435 nm probe light, but data were obtained for selected samples with other probe wavelengths throughout the transient absorption or bleach regions, and no significant wavelength dependence of the kinetics was observed. Because of the limited length of the optical delay line, kinetic data could only be measured to ≈500 ps. A check of the alignment of the optical delay line was performed by replacing the MbNO sample with MbCO, which is expected to yield a decay free transient over the 500 ps range.

3. Results

The absorption spectrum of MbNO consists of weak Q-band absorptions in the 550 nm region and an intense Sorét band absorption near 420 nm. Following excitation of MbNO with a 570 nm pulse, the Sorét band absorption maximum undergoes a transient shift to longer wavelength, reflecting photolysis of the NO ligand. In the difference absorption spectrum (photolyzed minus unphotolyzed) this photolysis leads to a negative feature (bleach) near 420 nm and a positive feature (increased absorption) near 435 nm (see Figure 1). As can be seen from the data shown in Figure 1, and has been verified quantitatively for several samples (vide supra), there is minimal spectral evolution of this difference spectrum during the time scale of ligand rebinding. This result indicates that the recovery kinetics can be followed by measuring the amplitude of the difference spectrum at any convenient wavelength in this spectral region. In Figure 2, the dynamics of NO recombination, monitored with a probe wavelength of 435 nm, are presented for glycerol concentrations ranging from 0 to 90% (w/v) in buffer. Each trace is obtained from the average of at least three independent experiments performed on at least two different samples.

4. Discussion

As is well known, the dynamics of diatomic ligand rebinding to the heme group in Mb cannot be described by a single

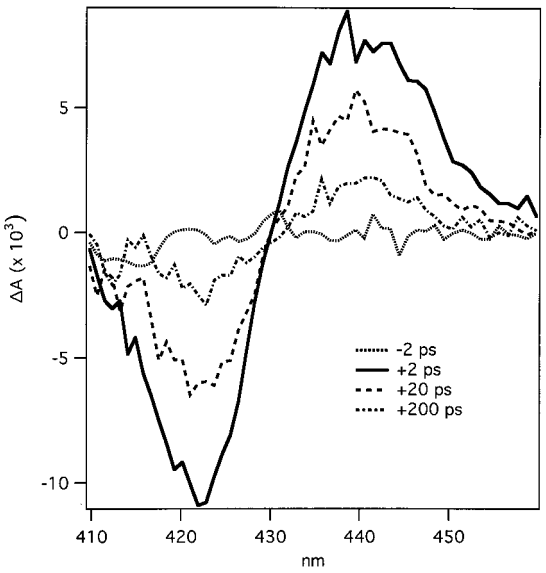

Figure 1. The difference spectrum obtained from MbNO as a function of delay time following photolysis. The positive peak near 440 nm results from the Sóret band absorption of deliganded Mb, formed upon photolysis, whereas the negative peak near 422 nm results from the disappearance of the Sóret band absorption of MbNO.

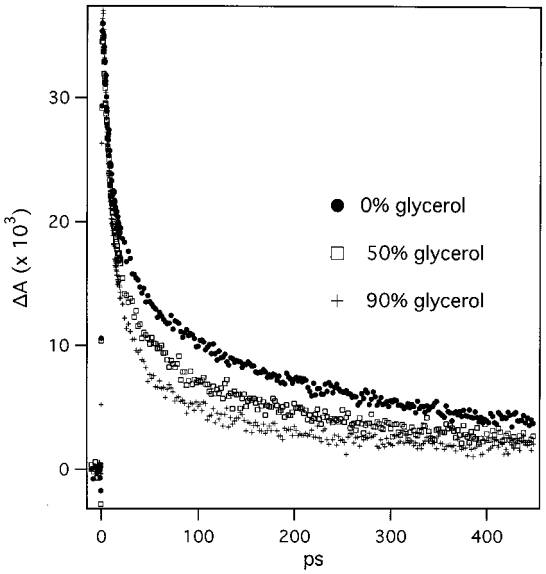

Figure 2. Time dependence of the differential absorption signal measured at 435 nm following photolysis of MbNO. Data are shown for three different glycerol concentrations (w/v) in buffer. The negative signal at extremely early times results from a cross-phase modulation contribution.

exponential. This situation is apparent from any of the curves plotted in Figure 2, each of which is clearly nonsingle exponential. In attempting to analyze data that are not well fit by a single exponential decay, the issue arises as to the uniqueness of the model. In this work, we have taken the approach of applying maximum entropy analysis to determine the least structured distribution of rate processes (vide infra) that is required to fit each data set to within the noise present in the data. As discussed later, the application of maximum entropy analysis suggests that at least two distinguishable rate processes, each of which may be distributed, are required to analyze the kinetic data. The interpretation of the data is presented in terms of likely physical processes associated with these rate processes. In addition to the maximum entropy approach, we note empirically that a plot of the data on a log−log scale also indicates the presence of two distinct rebinding phases as opposed to, for example, a stretched exponential process.[16]

Once the presence of two distinct rebinding processes is identified, the fitting could of course proceed by use of simple least-squares minimization methods using a double exponential decay function. Indeed, we have also carried out such fits as described later. However, in the present work, the use of the maximum entropy approach is preferred for a number of reasons. First, the maximum entropy method naturally incorporates the possibility that one or both of the rebinding processes might demonstrate distributed kinetics, due for example, to an inhomogeneous distribution of populations. Second, in direct contrast to simple least-squares minimization procedures, the maximum entropy approach automatically avoids data overfitting, that is, fitting noise as well as data. A third, related, point is that the maximum entropy approach also provides protection against overinterpretation of the data. This occurs because the distributed width of a kinetic process obtained from the maximum entropy method reflects the signal-to-noise ratio of the data (with noisier data resulting in wider distributions) in addition to any intrinsic width due to actual distributed kinetic processes. Therefore, the maximum entropy approach avoids interpreting data in terms of multiple exponential processes that are, in fact, unresolvable from a single distributed process for the given signal-to-noise level.

The maximum entropy method has been used previously for analyzing rebinding kinetics of Mb and is only briefly described here.[7,16−18] The general approach takes the observed signal, $y(t)$, to be represented by a distribution of rate processes, as in

$$y(t) = \int \mathrm{d}k\, g(k)\, \mathrm{e}^{-kt} + \Delta(t) \qquad (1)$$

where $g(k)$ is the amplitude distribution of rates k and $\Delta(t)$ represents noise. Because of the presence of noise, the inverse Laplace transform required to determine $g(k)$ from the observed data $y(t)$ is not unique. The maximum entropy algorithm leads to the determination of the particular $g(k)$ that reproduces the data to the level of the noise (i.e., $\chi^2 \approx 1$), while at the same time having the maximum value for the entropy function

$$S = -\int \mathrm{d}k\, g(k) \ln\{g(k)/w(k)\} \qquad (2)$$

In eq 2, the distribution $w(k)$ represents the prior distribution, which in the absence of any information is taken to be uniform on a logarithmic scale.[7,16,18] In a physical sense, this implementation of the maximum entropy method guarantees that any structure imposed upon the distribution $g(k)$ is required by the data, for in the absence of any requirement from the data, $g(k)$ will be structureless.

A key component to obtaining reliable results from a maximum entropy approach is that the noise in the data must be accurately estimated. To ensure that the noise was not underestimated, several tests were routinely performed.[7] First, the noise was estimated by choosing portions of each data set and calculating the root mean square (rms) deviation of the data from a smooth polynomial fit through the data. Another estimate was made by fitting the data to a large number of exponential decays and then calculating the rms of the residuals from this smooth fit. Finally, the maximum entropy method could be run with a lower and lower estimate of noise until the data were fit to flatness, and the rms of the residuals from that fit were calculated. All of these approaches gave similar estimates for each data set, and in practice, to avoid overfitting of the data, the maximum entropy method was implemented with the noise

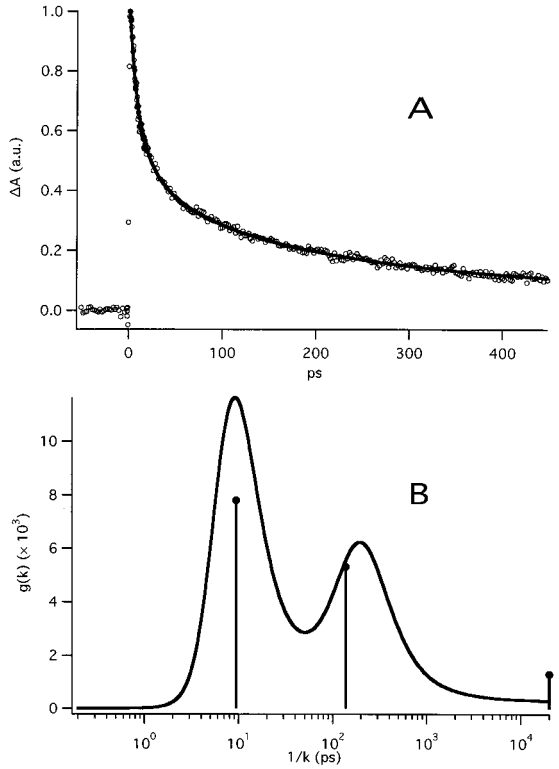

Figure 3. (A) The diffferential absorption data obtained with a probe wavelength of 435 nm in buffer solution (symbols) and the fit obtained using a maximum entropy analysis (line). (B) The maximum entropy method distribution of rates corresponding to the fit in the upper panel (curve) and the relative amplitudes obtained from a fit using two independent single exponentials plus a baseline (bars). The baseline amplitude is indicated by the bar to the extreme right.

taken to be at least 20% greater than the noise obtained from fits to flatness. In addition, it was verified that the general form of the distribution function determined by the maximum entropy calculation was unchanged by small variations in the estimated noise.

An example of a maximum entropy analysis of an MbNO data set is presented in Figure 3. This particular data set is that obtained from monitoring the recombination dynamics of NO in buffer solution. The maximum entropy analysis generates a distribution that contains two major peaks, one corresponding to a rate of ≈9.1 ps and the other corresponding to a rate of ≈200 ps, which is very similar to the distribution obtained in a previous study of NO recombination in sperm whale myoglobin.[7] Also, for comparison, the results of a nonlinear least-squares fit to the data assuming two exponential decay processes plus an offset to model the absence of complete recombination on the nanosecond time scale are shown. This comparison provides a useful check, although as already noted, the maximum entropy method is preferred for much of the remainder of the data analysis. The distributions *g(k)* determined for each of the data sets shown in Figure 2 are presented in Figure 4. There is a profound dependence of the distribution functions on glycerol concentration. The primary effect of increasing glycerol content is that the amplitude of the slower rate process is decreased, along with a concomitant increase in its rate, whereas the amplitude of the faster process increases with no significant change in rate. The remainder of the discussion centers on how to understand these changes within the framework of simple models of the observed kinetics.

A number of experimental techniques have shown that in MbCO, at either ambient or cryogenic temperatures, the

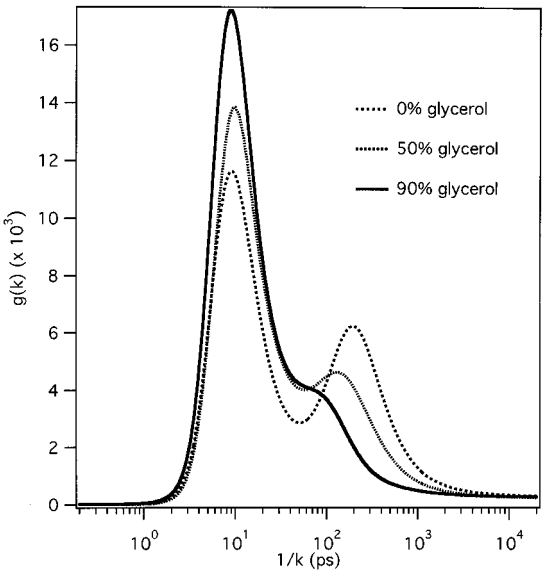

Figure 4. The dependence of the maximum entropy distributions on the concentration of glycerol (w/v) for NO recombination following photolysis of MbNO.

photodissociated CO molecules quickly move to a so-called docking site that is within the distal pocket and quite near the heme group.[2,19−22] Broadly speaking, these previous experiments can be placed into three categories. First, numerous spectroscopic studies (see, for example, Ansari et al.[2]) of cryogenically trapped intermediates and the temperature dependence of their rebinding processes have indicated the presence of structurally (and spectroscopically) distinct populations of photolyzed CO, still within the protein. Second, X-ray crystallography of both a cryogenically trapped photolysis intermediate[20] and a transient, ambient-temperature intermediate[21] has demonstrated the presence of a distinct binding site for the photolyzed CO near the heme group. Finally, ambient-temperature, time-resolved IR spectroscopy of MbCO in solution has demonstrated that the vibrational spectral signatures of the photolyzed CO at early times following photolysis are closely analogous to the spectral signatures observed at low temperature.[19,22] Comparison of the transient (or low temperature) IR data, including polarization analysis, and the corresponding crystallographic studies suggests that the primary spectrally distinct states of the photolyzed CO (the so-called B_1 and B_2 states) likely correspond to end-to-end isomers of the CO molecule within a single docking site. At room temperature, the IR spectral features that correspond to these populations of photolyzed CO appear within 200 and 500 fs following the excitation pulse.[19,22] A subsequent relaxation process occurs within ≈1.6 ps, yielding spectral features that are stable until interconversion between the two B states occurs on a time scale approaching 100 ps.[19,22]

In the case of MbNO, similar processes are presumed to occur following photodissociation. There is as yet no direct crystallographic structural evidence concerning the nature of photolyzed states for diatomic ligands other than CO. Recently, though, low-temperature IR spectroscopic studies have demonstrated the existence of two NO populations in the globin.[13] These data suggest that photodissociated NO is also found in docking sites near the heme iron, and that the geminate recombination process studied here occurs from these states. In fact, at low temperature (<35 K), the temperature dependence for the recombination of the individual NO subpopulations is indicative of two different barriers for recombination for the two states (hereafter referred to as B_1 and B_2 in analogy with

SCHEME 1

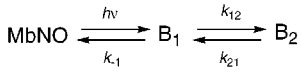

SCHEME 2

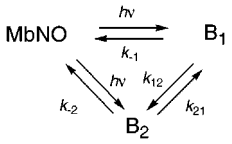

CO).[13] This observation, which parallels similar findings for CO recombination, is also consistent with the view that the kinetic data reported here are dominated by ligand recombination from two docking states in the distal pocket of Mb. All of our subsequent analysis is thus based on the assertion that the subnanosecond recombination dynamics in room-temperature MbNO reflect the dynamics associated with two distinct ligand docking sites. A key test of this supposition would be to monitor the time-resolved IR spectrum following photolysis of room-temperature MbNO, and determine if the distinct photolyzed NO states have dynamics that can be correlated with distinct processes in the rebinding kinetics.

The observed dynamics as a function of glycerol content provide specific constraints for kinetic models of dissociated ligand rebinding. Schematically, we will consider a model in which MbNO can be photodissociated to form two different states, denoted B_1 and B_2. Two possible kinetic schemes can be considered, namely, Scheme 1, a sequential model in which B_1 is the only initially populated state, and Scheme 2, a parallel model in which both B_1 and B_2 are initially populated by the photolysis event. Both models can be solved analytically and both lead to biexponential kinetics (see *Appendix*) of the following form:

$$y(t) = K_+ \exp(\lambda_+ t) + K_- \exp(\lambda_- t) \qquad (3)$$

However, examination of the solutions indicates that the sequential model predicts that K_+/K_- depends solely on the microscopic rate constants that also determine λ_+ and λ_-. Thus, for the sequential model to be correct, all of the primary rate constants must change simultaneously in just such a way that the rate of the fast process remains unchanged while its relative amplitude increases, and this balance must be maintained over the entire range of glycerol concentrations used here.[23] For all three primary rate constants in this model to change simultaneously in just such a way as viscosity is varied over >2 orders of magnitude and internal hydration changes associated with glycerol concentration occur would be a remarkable coincidence. In contrast, the parallel model provides an obvious mechanism for decoupling the observed rates and amplitudes through changing the initial branching ratio. For this reason, we favor the parallel scheme.[24] In this case, the data can be modeled with the following two simple assumptions: (1) changing glycerol concentration changes the initial partitioning between B_1 and B_2; and (2) the recombination rate of B_1 is independent of glycerol concentration, whereas the recombination rate of B_2 increases with increasing glycerol content.

We consider each of these assumptions in turn. A change in glycerol content of the buffer could easily perturb the initial partitioning of B_1 and B_2, either through a perturbation of ligand trajectories following photodissociation or through a change of the initial inhomogeneous ground-state distribution of protein conformations, each member of which might correlate with a specific photodissociated product. The influence of glycerol on the recombination rate of B_2 is also easily rationalized. If we adopt the interpretation that B_2 and B_1 are roto-isomers of one another, as in the case of CO (vide supra), then a likely recombination pathway for B_2 would involve conversion of B_2 to B_1, followed by fast rebinding from B_1 (i.e., $k_{21} \gg k_{-2}$ in Scheme 2). That this interpretation provides a reasonable recombination route is further supported by the observation that the interconversion of B_2 and B_1 populations for photodissociated CO at room temperature occurs on a time scale of between 10 and 100 ps, which approaches the rebinding kinetics of B_2 observed here.[19,22] An exact match would, of course, not be expected because the rotational barrier for NO following protein relaxation could differ slightly from that for CO. The primary difference between photodissociated NO and CO would then be that a large inner barrier for CO slows the rebinding from the B_1 state, whereas for NO this rebinding is quite rapid (the $\approx$10 ps process observed independent of glycerol concentration). Thus, the kinetic basis for the effect of glycerol on recombination rates would be that increased glycerol concentration leads to an increase in k_{21}, indicating a corresponding decrease in the energetic barrier between B_2 and B_1, which could arise from a change in either the structure or the stabilization of B_2 (via protein relaxation) on the time scale of the interconversion. Further examination could again be provided by time-resolved IR studies in which the structure and dynamics of each of the observable B states, including their rebinding and interconversion, could be followed and correlated with overall protein relaxation dynamics. A final interesting point is that within the model suggested here, the primary barrier to recombination for photodissociated NO arises from distal side effects (specifically from the barrier for B_2 to B_1 interconversion), which is consistent with many previous observations of distal side mutations influencing NO recombination.[9,25,26] In the case of photodissociated CO, the rebinding processes are additionally strongly influenced by the barrier for B_1 rebinding, which may also involve proximal side effects. This latter barrier is obviously very small for NO, given both the room-temperature rate of its fast rebinding process (this work), and the need to have the temperature <20 K to trap this intermediate state.[13] In addition, this inner barrier for NO rebinding is independent of glycerol concentration and so is decoupled from any protein relaxation process that is influenced by added glycerol.

Conclusions

The results of this study of the dependence of recombination of NO in horse Mb upon glycerol concentration, carried out on the ultrafast time scale in room temperature solutions, indicate that the photodissociated ligand partitions almost immediately into two populations that demonstrate different rebinding kinetics. We suggest that these populations correlate with the B_1 and B_2 states recently observed in low-temperature IR experiments on MbNO. Solution glycerol content changes the relative amplitude of these two populations either by influencing ligand trajectories or by perturbing a distribution of ground-state populations that might correlate with distinct photodissociated populations. One major conclusion is that modeling of the data requires the assertion that the recombination rate of the faster population (B_1) is independent of glycerol concentration, and therefore, independent of any protein relaxation process that is influenced by the addition of glycerol. In contrast, the recombination rate of the slower population (B_2) increases with increasing glycerol concentration. A likely structural interpretation, based on results from the study of MbCO, is that the two

states are roto-isomers of one another. In this case, the rebinding of the slower population presumably must involve the interconversion of B_2 and B_1, a process that has been observed for photodissociated CO to occur on similar time scales to those observed for the slow rebinding phase here. An increase in glycerol is then taken to lead to a lowering of the barrier between B_2 and B_1, which could either occur due to a change in the structure of B_2 or to a decrease in the energy stabilization of B_2 associated with protein relaxation. An experimental test of these interpretations and suppositions would be to perform an ultrafast, time-resolved IR absorption study of MbNO to correlate rebinding and relaxation kinetics with the time-dependent populations and structures of the distinct states observable in the IR spectrum.

Acknowledgment. We thank Dr. David Lambright for assistance in implementing the maximum entropy method used here. M.C.S. was supported by a Department of Energy Postdoctoral Fellowship. A.P.S. was supported by a J. Robert Oppenheimer Fellowship and S.F. was supported by a Director's Office Postdoctoral Fellowship, both from Los Alamos National Laboratory. This work was supported in part by National Institutes of Health Grant GM53640 (RBD).

Appendix

The sequential scheme (Scheme 1) is described by the following differential equations (where the time-dependent functions denote concentrations):

$$\mathrm{d/d}t\ \mathrm{MbNO}(t) = k_{-1}\,\mathrm{B}_1(t) \tag{A1}$$

$$\mathrm{d/d}t\ \mathrm{B}_1(t) = -(k_{-1} + k_{12})\,\mathrm{B}_1(t) + k_{21}\,\mathrm{B}_2(t) \tag{A2}$$

$$\mathrm{d/d}t\ \mathrm{B}_2(t) = k_{12}\,\mathrm{B}_1(t) - k_{21}\,\mathrm{B}_2(t) \tag{A3}$$

Equations A1−A3 are subject to the initial conditions

$$\mathrm{MbNO}(0) = 0 \quad \mathrm{B}_1(0) = \mathrm{B}^\circ \quad \mathrm{B}_2(0) = 0 \tag{A4}$$

where B° is the initial concentration of photolysis product. This set of equations can be solved, yielding

$$\mathrm{B}_1(t) = (\mathrm{B}^\circ/D^{1/2})\{(k_{21} + \lambda_+)\exp(\lambda_+ t) + (k_{21} + \lambda_-)\exp(\lambda_- t)\} \tag{A5}$$

and

$$\mathrm{B}_2(t) = ((k_{12}\mathrm{B}^\circ)/D^{1/2})\{\exp(\lambda_+ t) + \exp(\lambda_- t)\} \tag{A6}$$

where

$$D = (k_{-1} + k_{12} + k_{21})^2 - 4k_{-1}k_{21} \tag{A7}$$

$$\lambda_\pm = (1/2)\{-(k_{-1} + k_{12} + k_{21}) \pm D^{1/2}\} \tag{A8}$$

Because the change in molar absorptivities probe the ligation state of the heme Fe atom, the observed experimental signal is proportional to $\mathrm{B}_1(t) + \mathrm{B}_2(t)$, given by

$$\mathrm{B}_1(t) + \mathrm{B}_2(t) = (\mathrm{B}^\circ/D^{1/2})\{(k_{12} + k_{21} + \lambda_+)\exp(\lambda_+ t) - (k_{12} + k_{21} + \lambda_-)\exp(\lambda_- t)\} \tag{A8}$$

Equation A8 represents a biexponential decay of signal in which the observed rates (λ_+,λ_-) and the microscopic rate constants explicitly and solely determine the relative amplitudes of the two exponential components.

The parallel scheme (Scheme 2) is described by the closely related set of differential equations:

$$\mathrm{d/d}t\ \mathrm{MbNO}(t) = k_{-1}\,\mathrm{B}_1(t) + k_{-2}\,\mathrm{B}_2(t) \tag{A9}$$

$$\mathrm{d/d}t\ \mathrm{B}_1(t) = -(k_{-1} + k_{12})\mathrm{B}_1(t) + k_{21}\mathrm{B}_2(t) \tag{A10}$$

$$\mathrm{d/d}t\ \mathrm{B}_2(t) = k_{12}\,\mathrm{B}_1(t) - (k_{-2} + k_{21})\,\mathrm{B}_2(t) \tag{A11}$$

Equations A9−A11 are subject to the following initial conditions

$$\mathrm{MbNO}(0) = 0 \quad \mathrm{B}_1(0) = \mathrm{B}_1^\circ \quad \mathrm{B}_2(0) = \mathrm{B}_2^\circ \tag{A12}$$

where $\mathrm{B}_1^\circ + \mathrm{B}_2^\circ = \mathrm{B}^\circ$, the initial concentration of photolysis product. Solution of this set of equations yields

$$\mathrm{B}_1(t) = (1/D^{1/2})\{(k_{-2} + k_{21} + \lambda_+)(\mathrm{B}_1^\circ - ((k_{-2} + k_{21} + \lambda_-)/k_{12})\mathrm{B}_2^\circ)\exp(\lambda_+ t) - (k_{-2} + k_{21} + \lambda_-)(\mathrm{B}_1^\circ - ((k_{-2} + k_{21} + \lambda_+)/k_{12})\mathrm{B}_2^\circ\exp(\lambda_- t)\} \tag{A13}$$

and

$$\mathrm{B}_2(t) = (k_{12}/D^{1/2})\{(\mathrm{B}_1^\circ - ((k_{-2} + k_{21} + \lambda_-)/k_{12})\mathrm{B}_2^\circ) \times \exp(\lambda_+ t) - (\mathrm{B}_1^\circ - ((k_{-2} + k_{21} + \lambda_+)/k_{12})\mathrm{B}_2^\circ)\exp(\lambda_- t)\} \tag{A14}$$

where, now

$$D = (k_{-1} + k_{-2} + k_{12} + k_{21})^2 - 4\,(k_{-1}k_{-2} + k_{-1}k_{21} + k_{-2}k_{12}) \tag{A15}$$

and

$$\lambda_\pm = (1/2)\{-(k_{-1} + k_{-2} + k_{12} + k_{21}) \pm D^{1/2}\} \tag{A16}$$

As before, the observed signal will be proportional to $\mathrm{B}_1(t) + \mathrm{B}_2(t)$.

For this scheme, the relative amplitudes of the two exponential components are no longer solely dependent on the primary rate constants but also depend strongly on the ratio ($\mathrm{B}_1^\circ/\mathrm{B}_2^\circ$). Therefore, a change of this photolysis ratio can change the relative amplitudes even if the observed rate of the faster recombination process (λ_-) remains constant.

References and Notes

(1) Henry, E. R.; Sommer, J. H.; Hofrichter, J.; Eaton, W. A. *J. Mol. Biol.* **1983**, *166*, 443.
(2) Ansari, A.; Berendzen, J.; Braunstein, D.; Cowen, B. R.; Frauenfelder, H.; Hong, M. K.; Iben, I. E. T.; Johnson, J. B.; Ormos, P.; Sauke, T. B.; Scholl, R.; Schulte, A.; Steinbach, P. J.; Vittitow, J.; Young, R. D. *Biophys. Chem.* **1987**, *26*, 337.
(3) Findsen, E. W.; Ondrias, M. R. *Photochem. Photobiol.* **1990**, *51*, 741.
(4) Springer, B. A.; Sligar, S. G.; Olson, J. S.; Phillips, G. N. *Chem. Rev.* **1994**, *94*, 699.
(5) Chance, M. R.; Courtney, S. H.; Chavez, M. D.; Ondrias, M. R.; Friedman, J. M. *Biochemistry* **1990**, *29*, 5537.
(6) Petrich, J. W.; Poyart, C.; Martin, J. L. *Biochemistry* **1988**, *27*, 4049.
(7) Petrich, J. W.; Lambry, J. C.; Balasubramanian, S.; Lambright, D. G.; Boxer, S. G.; Martin, J. L. *J. Mol. Biol.* **1994**, *238*, 437.
(8) Walda, K. N.; Liu, X. Y.; Sharma, V. S.; Magde, D. *Biochemistry* **1994**, *33*, 2198.
(9) Gibson, Q. H.; Regan, R.; Elber, R.; Olson, J. S.; Carver, T. E. *J. Biol. Chem.* **1992**, *267*, 22022.
(10) Lim, M.; Jackson, T. A.; Anfinrud, P. A. *Proc. Natl. Acad. Sci. U.S.A.* **1993**, *90*, 5801.
(11) Causgrove, T. P.; Dyer, R. B. *J. Phys. Chem.* **1996**, *100*, 3273.
(12) Jackson, T. A.; Lim, M.; Anfinrud, P. A. *Chem. Phys.* **1994**, *180*, 131.

(13) Miller, L. M.; Pedraza, A. J.; Chance, M. R. *Biochemistry* **1997**, *36*, 12199.
(14) Miner, C. S.; Dalton, N. N. *Glycerol*; Reinhold Publishing: New York, 1953.
(15) Sastry, G. M.; Agmon, N. *Biochemistry* **1997**, *36*, 7097.
(16) Steinbach, P. J.; Chu, K.; Frauenfelder, H.; Johnson, J. B.; Lamb, D. C.; Nienhaus, G. U.; Sauke, T. B.; Young, R. D. *Biophys. J.* **1992**, *61*, 235.
(17) Skilling, J.; Bryan, R. K. *Mon. Not. R. Astron. Soc.* **1984**, *211*, 111.
(18) Lambright, D. G.; Balasubramanian, S.; Boxer, S. G. *Biochemistry* **1993**, *32*, 10116.
(19) Lim, M.; Jackson, T. A.; Anfinrud, P. A. *J. Chem. Phys.* **1995**, *102*, 4355.
(20) Schlichting, I.; Berendzen, J.; Phillips, G. N.; Sweet, R. M. *Nature* **1994**, *371*, 808.
(21) Srajer, V.; Teng, T.-y.; Ursby, T.; Pradervand, C.; Ren, Z.; Adachi, S.-i.; Schildkamp, W.; Bourgeois, D.; Wulff, M.; Moffat, K. *Science* **1996**, *274*, 1726.
(22) Lim, M. H.; Jackson, T. A.; Anfinrud, P. A. *Nat. Struct. Biol.* **1997**, *4*, 209.
(23) For example, if an analysis were carried out using relative amplitudes and rates corresponding to double exponential plus baseline fits to the data (used here instead of the maximum entropy approach to allow precise estimation of the amplitude of the long-time baseline; vide infra) and the full solution of the sequential kinetic model, the following result would be obtained. In buffer solution (0% glycerol), $k_{-1} = 0.061$ ps^{-1}, $k_{12} = 0.040$ ps^{-1}, and $k_{21} = 0.013$ ps^{-1}; whereas in the 90% glycerol solution, $k_{-1} = 0.075$ ps^{-1}, $k_{12} = 0.023$ ps^{-1}, and $k_{21} = 0.017$ ps^{-1}. Thus, k_{-1} would increase with increasing glycerol content (and viscosity), whereas the equilibrium between B_1 and B_2 would be shifted toward B_1 by an increase in k_{21} and a corresponding decrease in k_{12}. In all of the kinetic analyses discussed here, whether carried out using the results of a maximum entropy method or a fit to exponentials, an issue is how to treat the minor kinetic component that remains after the two larger amplitude recombination phases are complete. In the case where the data are fit to a biexponential plus baseline model, the relative amplitude of the baseline ranges from 0.09 for the 0% glycerol solution to 0.05 for the 90% glycerol solution. The fundamental rate constants already presented were obtained by combining the relative amplitude of the slow kinetic phase and the baseline offset into a single amplitude used in combination with the slow kinetic rate. Another analysis was done in which the amplitude of the baseline offset was simply ignored, and the relative amplitudes of the fast and slow rate processes were renormalized to add to unity. This analysis leads to an ≈5% increase in k_{-1}, an ≈10% decrease in k_{12}, and an ≈5% decrease in k_{21}, but leaves the trends with respect to viscosity unaltered. For the analysis using the results of the maximum entropy method, the amplitude of the long-time recombination processes is much harder to estimate quantitatively but appears to be consistent with these values.
(24) In this context, a parallel scheme denotes a kinetic scheme in which the two photodissociated states are formed with amplitudes that can vary independently from the fundamental rate constants that describe their interconversion. This kinetic scheme is not meant to imply that the formation of the two states occurs truly instantaneously upon photodissociation. The photoexcitation processes indicated in Schemes 1 and 2 can include fast formation dynamics that lead to the observed photodissociated states, as long as these dynamics are substantially faster than the recombination dynamics. In MbCO, as noted, the formation dynamics leading to the photodissociated states have been determined to be subpicosecond.[19,22]
(25) Carver, T. E.; Rohlfs, R. J.; Olson, J. S.; Gibson, Q. H.; Blackmore, R. S.; Springer, B. A.; Sligar, S. G. *J. Biol. Chem.* **1990**, *265*, 20007.
(26) Quillin, M. L.; Li, T. S.; Olson, J. S.; Phillips, G. N.; Dou, Y.; Ikeda-Saito, M.; Regan, R.; Carlson, M.; Gibson, Q. H.; Li, H. Y.; Elber, R. *J. Mol. Biol.* **1995**, *245*, 416.